

UC Riverside

UC Riverside Previously Published Works

Title

Self-assembled cationic amphiphiles as antimicrobial peptides mimics: Role of hydrophobicity, linkage type, and assembly state

Permalink

<https://escholarship.org/uc/item/3qv682wg>

Journal

Nanomedicine Nanotechnology Biology and Medicine, 13(2)

ISSN

1549-9634

Authors

Zhang, Yingyue
Algburi, Ammar
Wang, Ning
et al.

Publication Date

2017-02-01

DOI

10.1016/j.nano.2016.07.018

Peer reviewed



Published in final edited form as:

Nanomedicine. 2017 February ; 13(2): 343–352. doi:10.1016/j.nano.2016.07.018.

Self-assembled cationic amphiphiles as antimicrobial peptides mimics: Role of hydrophobicity, linkage type, and assembly state

Yingyue Zhang, PhD^a, Ammar Algburi^{b,c}, Ning Wang^a, Vladyslav Kholodovych, PhD^{d,e,f}, Drym O. Oh^f, Michael Chikindas, PhD^{g,h}, Kathryn E. Uhrich, PhD^{a,*}

^aDepartment of Chemistry and Chemical Biology, Rutgers University, Piscataway, NJ, USA

^bDepartment of Microbiology and Biochemistry, Rutgers University, New Brunswick, NJ, USA

^cDepartment of Microbiology, Veterinary College, Diyala University, Baqubah, Iraq

^dOffice of Advanced Research Computing (OARC), Rutgers University, Piscataway, NJ, USA

^eDepartment of Pharmacology, Robert Wood Johnson Medical School, Rutgers University, Piscataway, NJ, USA

^fErnest Mario School of Pharmacy, Rutgers University, Piscataway, NJ, USA

^gSchool of Environmental and Biological Science, Rutgers University, New Brunswick, NJ, USA

^hCenter for Digestive Health, NJ Institute for Food, Nutrition and Health, New Brunswick, NJ, USA

Abstract

Inspired by high promise using naturally occurring antimicrobial peptides (AMPs) to treat infections caused by antimicrobial-resistant bacteria, cationic amphiphiles (CAs) were strategically designed as synthetic mimics to overcome associated limitations, including high manufacture cost and low metabolic stability. CAs with facially amphiphilic conformation were expected to demonstrate membrane-lytic properties and thus reduce tendency of resistance development. By systematically tuning the hydrophobicity, CAs with optimized compositions exhibited potent broad-spectrum antimicrobial activity (with minimum inhibitory concentrations in low $\mu\text{g/mL}$ range) as well as negligible hemolytic activity. Electron microscope images revealed the morphological and ultrastructure changes of bacterial membranes induced by CA treatment and validated their membrane-disrupting mechanism. Additionally, an all-atom molecular dynamics simulation was employed to understand the CA-membrane interaction on molecular level. This study shows that these CAs can serve as viable scaffolds for designing next generation of AMP mimics as antimicrobial alternatives to combat drug-resistant pathogens.

*Corresponding author at: Department of Chemistry and Chemical Biology, Rutgers University, Piscataway, NJ 08854, USA. keuhrich@rutgers.edu (K.E. Uhrich).

Conflict of interest statement: we claim no conflict of interest.

Appendix A. Supplementary data

Supplementary data to this article can be found online at <http://dx.doi.org/10.1016/j.nano.2016.07.018>.

Upcoming poster of abstract at meeting: August 21st, ACS national meeting 2016, Philadelphia.

Keywords

Antimicrobial peptides; Synthetic mimics; Self-assembly; Membrane disruption; Antimicrobial activity

Using antimicrobials for control of infectious diseases has been a common practice since the 1940s.¹ However, the emergence of multidrug-resistant bacteria due to overuse and misuse of antimicrobial agents has become a severe threat to public health.² Compared to conventional antibiotics which target a specific biochemical process (e.g., DNA synthesis, protein synthesis) or molecule (e.g., enzyme), naturally occurring antimicrobial peptides (AMPs), as part of innate immune defense, have received substantial interest owing to their broad-spectrum activities, minimum cytotoxicity, and unique cellular membrane targeting mechanism.³ This mechanism can reduce the tendency of resistance development from genetic mutation. Thus, AMPs hold great potential for treating microbial infections as antibiotics alternatives.⁴⁻⁶

Despite diverse primary peptide sequences and secondary structures displayed by AMPs, many share two characteristics: cationic residues and hydrophobic domains, resulting in their amphiphilic topology.⁴ Recent literature results suggest that the biological activities of AMPs mainly depend on their physico-chemical properties.^{4,7} The cationic charges are essential to promote electrostatic interactions with negatively charged bacterial membranes,⁸ while hydrophobic residues aid in subsequent insertion into the hydrophobic core of the membranes, leading to membrane disruption, cytoplasm leakage, and eventual cell death.⁹ However, intrinsic drawbacks are associated with AMPs, including low metabolic stability (i.e., susceptibility to proteolysis),¹⁰ high manufacture cost, and formulation difficulties; these limitations have precluded their translational into clinical settings.⁴

Inspired by natural AMPs, a variety of structurally diverse synthetic mimics with key physicochemical natures (i.e., cationic charges and amphiphilicity) have been investigated, such as peptidomimetics,^{11,12} polymers (e.g., cationic derivatives of polyacrylate,¹³ poly(norbornene),¹⁴ poly(arylamide)¹⁵), and oligomers.¹⁶ Although these synthetic analogues are relatively facile and inexpensive to prepare in large quantities, obtaining potent antimicrobial activity while retaining high selectivity towards microbes (i.e., minimum toxicity towards mammalian cells) remains a challenge.¹⁵

As the facially amphiphilic conformation has been demonstrated to be a key factor in AMPs' unique biological profiles,¹⁷⁻¹⁹ we designed cationic amphiphiles (CAs) with similar spatial arrangements in which hydrophilic and hydrophobic residues of AMPs segregate to opposing domains.¹³ Comparing with their monomeric analogues, cationic gemini amphiphiles (i.e., two cationic head groups, two hydrophobic tails) have well-documented antimicrobial applications due to their enhanced surface activity. Thus, two series of biscationic compounds, ether- and ester-linked CAs, were synthesized with tartaric acid backbones and flexible spacers between the cationic charges and the backbone (Figure 1), which allowed the hydrophilic ammonium moieties and hydrophobic alkyl arms to be folded on opposite faces of the backbone. The hydrocarbon arms were conjugated to the backbone via ether or ester linkages, enabling the exploration of linkage type's influence on CAs'

biophysical properties, which has not been fully established. While increasing hydrophobicity may elicit an increase in antimicrobial potency,²⁰ undesirable increases in hemolytic and cytotoxic activities have also been reported.^{16,21} Thus, the hydrophobicity of CAmS was systematically tuned by varying hydrocarbon arm lengths to achieve potent bacterial membrane-lysing activity while mitigating adverse effects.

Upon successful synthesis, CAmS were observed to readily self-assemble into different nanostructures in aqueous solutions. Their antimicrobial activity was evaluated against a panel of microbes, including both Gram-positive and Gram-negative bacteria. The observed structure – activity relationship correlated specific design parameters with antimicrobial efficacy as well as cytotoxicity. Their postulated membrane-lytic mechanism was validated via microscopy techniques and molecular dynamics simulations were employed to examine CAM-membrane inter-actions on molecular level.

Methods

Materials

All reagents and solvents were purchased from Sigma-Aldrich (Milwaukee, WI) and used as received unless otherwise mentioned. Di-*tert*-butyl L-tartrate²² and di-2-bocaminoethyltartramide²³ were prepared as previously published. Anhydrous dimethylformamide (DMF) was dried over 4 Å molecular sieves at room temperature at least overnight prior to use. N-Boc-ethylenediamine was purchased from Alfa Aesar (Ward Hill, MA). 1-(3-dimethylaminopropyl)-2-ethylcarbodiimide hydrochloride (EDC·HCl) was purchased from AK Scientific (Union City, CA). Silicon wafers were purchased from Ted Pella, Inc. (Redding, CA). For cell experiments, reagents include human buffy coats purchased from the New York Blood Center (Long Island City, NY), penicillin/streptomycin purchased from Lonza (Basel, Switzerland), Dulbecco's modified eagle medium (DMEM) and Vybrant® MTT ((3-(4,5-dimethylthiazol-2-yl)-2,5-diphenyltetrazolium bromide) cell proliferation assay kit purchased from ThermoFisher Scientific (Waltham, MA).

Synthesis and characterization of ether- and Ester-linked cationic amphiphiles

Detailed descriptions of synthetic procedures, characterization methods, and product chemical structure information can be found in the supplemental material.

Dynamic light scattering (DLS) and zeta potential measurements

DLS and zeta potential were measured using a NanoZS90 instrument (Malvern Instruments, Southboro, MA). Samples were dissolved in deionized (DI) water at 1 mg/mL and filtered using 0.45 µm polytetrafluoroethylene (PTFE) syringe filters before measurement. To determine micelle sizes, each sample was run at a 90° scattering angle in triplicate with 30 measurements per run at 25 °C. All size results based on intensity distribution are presented as mean ± standard deviation around the mean.

Critical micelle concentration (CMC)

The surface tensions (γ) of CAmS were measured using a Fisher Surface Tensiometer model 21 (Waltham, MA) at room temperature.²⁴ The platinum ring was rinsed with hexane,

methanol, and DI water followed by heating with a Bunsen burner before use. A stock solution of CAmS (5 mL) was transferred into a carefully cleaned vessel and γ was measured repeatedly at least three times until the variation was smaller than 0.2 mN/m. The amphiphiles were then diluted with an aliquot of DI water and γ was collected at different concentrations. The γ values were then plotted against the logarithm of CAm concentrations, and the inflection point was taken as CMC.

Bacterial cell culture

The bacterial strains used for antimicrobial assay included: *Staphylococcus aureus* (*S. aureus*) ATCC 13565, *Listeria monocytogenes* (*L. monocytogenes*) Scott A, *Pseudomonas aeruginosa* (*P. aeruginosa*) ATCC 15442, *Escherichia coli* (*E. coli*) O157:H7, and *Salmonella enterica* serovar typhimurium (*S. typhimurium*). From the frozen stock ($-80\text{ }^{\circ}\text{C}$), bacteria were inoculated into brain-heart infusion (BHI) agar (Becton Dickinson, Franklin Lakes, NJ) and propagated under aerobic conditions at $37\text{ }^{\circ}\text{C}$ for 24 h. After the incubation, one colony of each bacterial strain was transferred separately to BHI broth (Becton Dickinson, Franklin Lakes, NJ) and incubated under aerobic condition at $37\text{ }^{\circ}\text{C}$ for 18–24 h. For broth microdilution assay, the bacterial growth suspensions were further diluted in fresh BHI medium to achieve 10^6 CFU/mL.

Broth microdilution assay

The minimal inhibitory concentration (MIC) of CAmS was identified using a broth microdilution assay modified from previous studies.²⁵ Briefly, fresh stock solutions of CAmS were prepared by dissolving in double-distilled water (ddH_2O) and sterilized under UV light for 25 min. The stock solutions were serial 2-fold diluted into a 96-well microplate (Becton Dickinson, Franklin Lakes, NJ) with BHI broth with a final volume of 100 μL . Aliquots (100 μL) of bacterial suspensions were added to each well of the microplate. Plates were incubated at $37\text{ }^{\circ}\text{C}$ for 24 h under aerobic conditions. The optical density readings of the microorganism at 595 nm were tracked using a microplate reader (Model 550, Bio-Rad Laboratories, Hercules, CA). The MIC was determined as the lowest CAm concentration that produced no visible growth after overnight incubation.

Scanning electron microscopy (SEM)

Bacteria were grown to the mid-exponential growth phase. Silicon wafers were submerged in the bacterial solutions in the presence or absence of CAmS at their respective MICs and incubated for 1 h. Glucose (0.25%) was added to facilitate attachment. The bacteria on wafers were fixed in 2.5% glutaraldehyde for 1 h at room temperature, washed three times with PBS, and post-fixed 1% osmium tetroxide. The samples were then dehydrated in a graded series of ethanol solutions (50%, 70%, 80%, 95%, 100%), dried with graded hexamethyldisilazane (50%, 100%), and air-dried for two days at room temperature. After drying, the wafers were mounted on stubs and sputter-coated with 20 nm gold prior to inspection under the microscope (Zeiss Sigma Field Emission SEM, Carl Zeiss, Ontario, CA) at 5 kV.

Transmission electron microscopy (TEM)

For micelle samples, a drop of the micelle solution was deposited onto on a carbon film-coated copper grid. After 60 seconds, excess solution was removed with filter paper. A drop of 1% uranyl acetate solution was then applied to the same grid for 60 seconds. The grid was again tapped dry and further dried in the desiccator overnight. For bacteria samples, bacteria were grown as described above for SEM sample preparation. In brief, bacteria were incubated in the presence or absence of CAmS at their respective MICs for 1 h. After centrifugation at $500\times g$ for 10 min, the resulting pellet was fixed in 2.5% glutaraldehyde, washed three times with PBS, and postfixed with 1% osmium tetroxide. The samples were then dehydrated with graded ethanol series (50%, 70%, 80%, 95%, 100%) and embedded in epoxy resin (Dr. Spurr's kit, Electron Microscopy Sciences, Hatfield, PA). Ultrathin sectioning of the cells was stained with 1% uranyl acetate. The microscopy was performed with JEOL 1200EX electron microscope (JEOL USA, Inc., Peabody, MA) at 80 kV.

Hemolytic activity

Hemolytic activity was determined following a modified procedure in literature.²⁶ Human red blood cells (hRBCs) were isolated from 7 mL human blood samples by centrifuging at $400\times g$ for 10 min (Allegra 21 centrifugation, Beckman Coulter, Brea, CA) to remove the plasma and buffy coat. The remaining pelleted RBCs were then washed with 15 mL sterile PBS five times and the supernatant was carefully removed using a pipette.

CAm stock solutions were prepared by dissolving CAmS in ddH₂O prior to use; the samples were gently agitated at 37 °C for 5 min until completely dissolved. To examine the hemolysis properties of CAmS, RBCs were suspended with PBS (5% hematocrit). Then 100 μ L of the suspended RBCs was mixed with 400 μ L freshly prepared CAm stock solutions with final concentrations of 7.8, 15.6, 31.2, 62.5, 125, and 250 μ g/mL. Additionally, ddH₂O water and PBS (400 μ L) were incubated with 100 μ L RBC suspension, serving as positive and negative controls, respectively. All the mixtures were gently shaken and incubated at 37 °C for 1 h. The mixtures were centrifuged at $400\times g$ (Labnet Spectrafuge 16 M microcentrifuge, Labnet International, Inc., Edison, NJ) for 10 min. The supernatant (100 μ L) was then transferred to a 96-well plate, and the absorbance (Abs) measured at 541 nm using an Infinite M200 PRO plate reader (Tecan Group Ltd., Männedorf, Switzerland). The following formula is used to calculate the percent of hemolysis of RBCs: $\text{hemolysis \%} = \frac{(\text{Abs}_{\text{sample}} - \text{Abs}_{\text{PBS}})}{(\text{Abs}_{\text{ddH}_2\text{O}} - \text{Abs}_{\text{PBS}})} \times 100$. HC₅₀ was defined as concentration required to induce 50% leakage of hemoglobin from hRBCs.

Human foreskin fibroblast (HFF) cell culture and MTT assay

HFFs were cultured in DMEM supplemented with 10% fetal bovine serum, 1% penicillin/streptomycin and plated at a concentration of 10,000 cells/well in 96-well plate. Plates were incubated at 37 °C and 5% CO₂ for 24 h to allow cell attachment prior to use. HFF is a well-accepted cell line to test general cytotoxicity of materials on mammalian cells.^{27,28}

CAmS were tested for cytotoxicity against HFFs using a tetrazolium-based colorimetric assay (MTT). CAmS were first dissolved in ddH₂O and then diluted in DMEM supplemented with 1% penicillin/streptomycin to reach concentrations of 3.9, 1.9, and 0.95

$\mu\text{g/mL}$. Cell media (100 μL) containing CAmS were then added to allocated wells in a 96-well plate. 1% Triton X-100 and cell medium only treated cells were used as positive and negative controls, respectively. After 24 h incubation, the medium was removed and replaced with fresh medium. MTT reagent (10 μL , 12 mM in PBS) was then added to each well and further incubated for 4 h at 37 °C. Formazan crystals were subsequently dissolved in 100 μL SDS solution (acidified with 0.01 M HCl) at 37 °C for 4 h. The absorbance (Abs) was then recorded with an Infinite M200 PRO plate reader (Tecan Group Ltd., Männedorf, Switzerland) at 570 nm. The following equation was used to calculate the percent of cell viability of HFFs: $\text{cell viability \%} = [(\text{Abs}_{\text{sample}} - \text{Abs}_{\text{Triton}})/(\text{Abs}_{\text{Medium}} - \text{Abs}_{\text{Triton}})] \times 100$.

Molecular dynamics simulations

Membrane patches of roughly $100 \times 100 \text{ \AA}$ were constructed with CHARMM-GUI web portal. The mammalian membrane top leaflet consisted of 147 POPC (1-palmitoyl-2-oleoyl-*sn*-glycero-3-phosphocholine) while the bottom leaflet was an equal mixture of POPE (1-palmitoyl-2-oleoyl-*sn*-glycero-3-phosphoethanolamine) and POPS (1-palmitoyl-2-oleoyl-*sn*-glycero-3-phospho-L-serine) molecules (84:84). Bacterial membrane had a mixture of 126 POPE and 42 POPG (1-palmitoyl-2-oleoyl-*sn*-glycero-3-phospho-(1'-*rac*-glycerol)) molecules in both leaflets. Membrane minimization and equilibration were performed with established protocols.²⁹ Details can be found in Supplemental Information.

5b in its extended conformations was rigidly docked in MOE program on the surface of equilibrated membrane patches obtained after 20 ns of molecular dynamics (MD) simulations. CAM-membrane assemblies generated were selected for further modeling by visual inspection based on two criteria: the distance between any atom of *5b* and the membrane should not exceed 5 \AA ; there was no initial penetration of any atom of *5b* into the membrane.

To probe the interaction between CAmS and membranes, MD program suite Amber 14 was used.^{30,31} Two separate systems were created, one with a mammalian membrane and one with a bacterial membrane. Each system was prepared by solvating it in water and neutralizing with sodium ions as needed with auxiliary preparation programs from AmberTools 15. After initial minimization, heating, and equilibration totaling 2 ns, *5b*-membrane assemblies were subjected to MD simulations for 50 ns. An isothermal-isobaric ensemble with Langevin thermostat and Berendsen barostat was used throughout MD simulations with restart checkpoints every 1 ns. Trajectory files from each 1 ns checkpoint step of MD simulations were collected and used for obtaining an averaged structure for every 1 ns with a modified subroutine from Visual Molecular Dynamics program. Thus, for each CAM-membrane assembly 50 averaged structures were calculated and compared. All calculations were performed on GPU enabled Linux cluster from OARC, Rutgers University.

Results

Synthesis and characterization of CAmS

Ether-linked CAmS were synthesized by alkylating di-*tert*-butyl L-tartrate (*1*) with bromoalkane through a nucleophilic substitution reaction and subsequently using TFA to deprotect the *tert*-butyl groups (Figure 1). The robust stability of *tert*-butyl groups in the presence of base allowed high alkylation yields (~50–60%).²² N-Boc-ethylenediamine was then incorporated to the resulting diacid (*3*) via carbodiimide coupling to generate CAm precursors (*4*). Following successful conjugation, *4* was deprotected using HCl in dioxane to afford the final product (*5*) as chloride salt with quantitative yields. The successful synthesis of all intermediates and CAmS was confirmed by NMR, FT-IR spectroscopies, and mass spectrometry.

Similarly, a series of CAmS with ester linkages between the hydrophobic arms and tartaric acid backbone was synthesized with analogous molecular weights, cationic net charge, and hydrophobicity (i.e., carbon numbers). Instead of alkylation, carbodiimide coupling was carried out with di-2-bocaminoethyltartramide and alkanic acids followed by acid-catalyzed deprotection to afford *8*. Both steps have yields higher than 80% and the chemical structures of all amphiphiles and intermediates were confirmed as described above for the ether-linked CAmS.

Self-assembly of CAmS

In water, all CAmS with the exception of *5a* and *8a* readily self-assembled into supramolecular nanostructures upon direct dissolution at their respective CMCs, ranging from 4 to 110 $\mu\text{g/mL}$. No stable self-assembled structures were observed for *5a* or *8a*, which had hydrophobic arms of only eight carbons, even at concentration as high as 1 mg/mL; thus, these two compounds were not further investigated. In comparing *8* to their respective ether counterparts (*5*), all ester-linked CAmS exhibited CMC values approximately 4–5 fold lower than their analogous ether-linked CAmS.

The micelle sizes were then determined by DLS while overall net charges characterized by zeta potential (Table 1). All materials formed nanoscale micelles with sizes between 50 and 100 nm with positive potentials ranging from 21 to 45 mV. The morphology of micelles was examined via TEM, and it was evident that spherical micelles were spontaneously formed (Figure 2).

Antimicrobial activity

CAmS were subsequently evaluated against five selected pathogenic microorganisms, including Gram-positive bacteria (i.e., *S. aureus* and *L. monocytogenes*) and Gram-negative bacteria (i.e., *E. coli*, *S. typhimurium*, and *P. aeruginosa*), using a turbidity-based microdilution method. MICs were taken as the lowest concentrations that completely inhibited bacteria growth. As shown in Table 2, CAmS showed antimicrobial activity against a panel of Gram-positive and Gram-negative bacteria. In addition, the CAmS were biologically more active against Gram-positive bacteria than Gram-negative bacteria with the MIC values being 2 to 4-fold lower.

Notably, the most hydrophobic CAmS with longest alkyl chains (*5c* and *8c*) did not show appreciable antimicrobial activity even at the highest concentration (250 µg/mL) tested. However, CAmS with shorter alkyl lengths demonstrated remarkably enhanced antimicrobial efficiency. In particular, *5b* and *8b*, with intermediate arm length, demonstrated the most superior antimicrobial activity with MIC values as low as 0.95 and 3.9 µg/mL for Gram-positive and Gram-negative bacteria, respectively. In addition, CAmS with ether linkages (*5*) exhibited greater antimicrobial efficacy than ester-linked counterparts (*8*).

Cell compatibility

A hemolysis assay was conducted by incubating hRBC with CAmS at various concentrations. Selectivity indices (SI) were determined as HC_{50}/MIC using *S. aureus* and *E. coli* as representatives for SI calculations of G+ and G– respectively. In general, all CAmS induced negligible hemolysis at their respective MICs (Figure 3, A), though the ether series displayed higher SI towards bacterial cells over mammalian cells.

Non-bioactive *5c* and *8c* as induced the lowest hemolytic response ($HC_{50} > 250$ µg/mL), revealing their low membrane activity overall. The CAmS *5a* and *8a* with a side-chain length of eight carbons demonstrated sufficiently high HC_{50} values (47 and 139 µg/mL) but with moderate selectivity (i.e., 2–12 fold). In particular, antimicrobial agents *5b* and *8b* preferentially interacted with bacterial cells and exhibited the highest selectivity. Compound *5b* showed slightly better performance compared to its ester analog *8b*, with SI as high as 68 for Gram-positive bacteria and 17 for Gram-negative bacteria as opposed to SI values of 43 and 11.

To further examine the biocompatibility of lead CAmS, cytotoxicity was determined after co-incubation with HFFs for prolonged time at MIC levels, followed by quantification of cell viability. Compounds *5b* and *8b* did not induce any pronounced cytotoxicity to cells at concentrations sufficient to inhibit microbial growth (Figure 3, B). The lead antimicrobial *5b*, which exerted the most potent antimicrobial activity while having the highest selectivity, was selected for further mechanistic study.

Mechanism of action

To validate the proposed membrane-targeting mechanism of CAmS, *S. aureus* and *E. coli* were selected from Gram-positive and Gram-negative bacterial strains, respectively. Bacteria were treated with the lead antimicrobial *5b* at its MIC levels. Significant morphological and ultrastructural alternations in comparison to the control (untreated bacterial cells) were observed with SEM and TEM.

Control cells (Figure 4, A and C) in SEM images appeared intact with smooth and well-defined surfaces, whereas treated cells showed severe membrane deformation. Open holes, deep craters, and protruding bumps (Figure 4, B) were observed with *S. aureus* treated with *5b*. Furthermore, burst cells and cellular debris of *S. aureus* were seen. However, for treated *E. coli* cells (Figure 4, D), minor blisters and bumps formed on the surface, which required further evidence from TEM images.

TEM was then used to examine ultrastructural changes in bacteria induced by CAmS. Prior to treatment, *S. aureus* showed regular round cells with intact and smooth surfaces (Figure 5, A). In addition, the intracellular DNA region displayed a heterogeneous electron density. However, upon treatment with *5b*, the bacteria showed profound internal damage, aside from cell membranes disruption (Figure 5, B).^{32,33} Multiple spherical void structures were observed, as well as cytoplasm with a more uniform electron density. Initially, *E. coli* displayed normal rod shape and undamaged cell membrane structure (Figure 5, C). On the contrary, treated *E. coli* experienced extensive ultrastructural damage and showed strong evidence of membrane disruption and rupture (Figure 5, D). Periplasmic space was expanded and had an irregular course. The polar regions of the cells even experienced fragmentation.

MD simulation

All-atom MD simulation was applied to elucidate the interactions between CAmS and membranes. We constructed a neutral bilayer to mimic a mammalian cell membrane with POPC as the top leaflet and mixture of POPE/POPG (1:1) as the bottom leaflet.³⁴ A mixture of anionic lipids POPE/POPG (3:1) in both leaflets was used to mimic the main components of a bacterial cell membrane.³⁵

Lead compound *5b* was selected and rigidly docked on the surface of membranes; followed by MD simulation for up to 50 ns. MD trajectories were collected and averaged structures of CAM-membrane ensembles were calculated for every 1 ns. Preferable interaction pattern for *5b* was clearly observed with negative charge bearing bacterial membrane (Figure 6, B) compared to neutral mammalian membrane (Figure 6, A). The insertion of one alkyl arm of *5b* into bacterial membrane happened within 1 ns of simulation and retained with much deeper penetration throughout the entire simulation (Figure S1). Even more striking difference was observed at the more advanced stages of MD simulation, where around 42 ns the second alkyl arm of *5b* got penetrated into bacterial membrane (Figure S2). Contrarily, *5b* adopted a more extended conformation on the surface of mammalian membrane within one hydrophobic arm remained in the water phase throughout the time.

Notably, *5b* adopted a facially amphiphilic conformation in the membrane-bound state with the bacterial membrane (Figure 6, B, $t = 50$ ns). At 20 ns, the tartaric acid backbone appeared to be parallel to the membrane surface, with ammonium groups localized at the water-membrane interface and one alkyl arm buried into the membrane hydrophobic core. With longer simulation, the cooperative electrostatic and hydrophobic interactions facilitated the other hydrophobic arm of *5b* to rearrange and project into the hydrophobic membrane environment, leading to efficient disruption of the bacterial membrane.

Discussion

Taking a biomimetic approach, we designed and synthesized two series of biscationic amphiphiles as AMP mimics which self-assembled into spherical nanostructures in aqueous solutions. As hydrophobicity is a key design parameter that can be tuned to obtain balance between antimicrobial activity and selectivity,^{21,36} CAmS with ester and ether linkages were synthesized with different hydrocarbon lengths. In previous work, we demonstrated that

replacing ester linkages with more flexible ether linkages in amphiphilic polymers dramatically affected their self-assembling behavior and molecular conformation, and ultimately changed their biological activities.³⁷ Thus, the linkage type was also varied in this study.

Dong et al reported substantially different biological profiles for fibrous cationic peptides and monomeric peptides, indicating the potential influence of assembling state on bioactivity.^{11,38} To establish the relationship between supramolecular structures and antimicrobial potency, the aggregation behavior of CAMs was carefully evaluated. The CMC discrepancy between the ether- and ester- linked series was appreciable, despite differing only by linkage type. The lower CMCs of ester-linked CAMs indicated their higher propensity to remain in an assembled state upon dilution. As expected, CMCs are dependent on the hydrophobicity of the alkyl arms, with increased hydrophobicity (from alkyl arm *c* to *a*) giving sequentially lower CMC values.³⁹

Higher MIC values of Gram-negative bacteria could be attributed to the presence of an additional lipopolysaccharide layer, which forms a hydrophilic barrier preventing hydrophobic CAMs from penetrating the membrane. In comparing amphiphiles' antibacterial activity, it became apparent that hydrophobicity, varied by alkyl chain length, significantly modulated their antimicrobial potency. No linear dependence on hydrophobicity was observed for HC₅₀ of CAMs. This result is surprising, considering that increased hydrophobicity has been correlated to stronger hemolytic activity.²⁰ MICs of *5b* and *8b* with intermediate arm length are amongst the lowest reported MIC values in the literature, especially in comparison to other gemini-type amphiphiles, such as bis-dimethylammonium bromide.^{40,41} Meanwhile, they demonstrated highest SI values and negligible cytotoxicity at concentrations high enough to inhibit bacteria growth, which is highly desirable for practical infection treatment. Given that a sufficient degree of hydrophobicity in the arms is required to promote intercalation and disruption of the bacterial membranes, these results indicated that a "sweet spot" in hydrophobicity was attained and conferred optimal antimicrobial activity and selectivity.^{16,21}

The disparity in antimicrobial activity between the two series likely stems from two reasons: (1) different flexibility of ether and ester linkages;²² (2) enhanced metabolic stability of ether linkage due to lack of enzymes capable of cleaving ether bond.³⁷ Considering that the presence of the carbonyl functionality in the hydrophobic domains of *8* limits the rotational flexibility of alkyl arms, we speculate that the flexible conformation of *5* increases the propensity of the hydrophobic chains to embed into and disintegrate the hydrophobic regions of lipid membranes; this hypothesis is currently under investigation via MD simulation. It is worth noting that the MICs of CAMs (except for non-bioactive *5c* and *8c*) are far below their respective CMCs, suggesting that it is the monomeric CAMs rather than the resulting self-assembled structures that enable the bioactivity. It is plausible that the stable nanostructures formed by *5c* and *8c* largely limit the interaction between the individual molecules and bacteria, which remarkably diminishes their affinity to bacterial membranes.^{21,42,43}

Taken together, two lead antimicrobials *5b* and *8b* displayed potent broad-spectrum antimicrobial activity while maintaining high cytocompatibility. Hydrophobicity is necessary

but not sufficient to dictate CAM's biological profiles, as linkage type and assembly state also play important roles in their behaviors.

From the combined evidences of SEM and TEM, it can be inferred that CAMs possess antimicrobial activity with membrane-disrupting mechanism, which is highly desirable as antibiotic alternatives to reduce resistance development in bacteria. The primary phospholipids in the outer leaflet of mammalian cell membranes are zwitterionic PC lipids while anionic PG lipids are rich in bacterial membranes.⁴⁴ The difference in membrane composition between bacteria and mammalian cells may account for the specificity and selectivity of CAMs, which was supported by our full atomistic MD simulation results.

Several prevailing models for the interaction of AMPs with the membranes, such as "barrel stave", "toroidal pore", "carpet model", and detergent model have been postulated.⁴⁵ While barrel-stave and toroidal pores models involved the formation of pores or channels through the membrane, AMPs can also intensively adsorb onto the surface and insert into the membrane to induce change in membrane permeability and integrity (carpet model) or act as detergents to extract lipids from the membrane.⁴⁶ The average thickness of the solvated and equilibrated POPE/POPG bilayer prior to CAM docking was found to be 43–45 Å. In comparison, the theoretical length for the fully stretched conformation of *5b* is about 24 Å, with a single hydrophobic arm being around 10–12 Å, which is unlikely to span the lipid bilayer and damage bacterial cell membrane through the pore formation models. We hypothesize the antimicrobial mechanism of CAMs is more likely the "carpet model" in which AMPs are attracted to membrane surface via electrostatic effects followed by insertion into the membrane.

The flexible ether linkage allows this conformational reorientation, likely contributing to the potent bioactivity of ether-linked CAMs. During this process, ammonium groups likely form a complex with negatively charged lipid head groups by a combination of electrostatic and hydrogen bonding effects, which has been previously observed.¹³

In summary, by fine-tuning the hydrophobicity, lead CAMs with potent broad-spectrum antimicrobial activity and desirable safety profiles were identified. Additionally, linkage type and assembly state were identified to be key determinants for optimal antimicrobial efficacy. Our molecules hold great promise to combat drug-resistance pathogens and are currently under investigation to eradicate biofilms with promising results, which will be reported in future works.

Supplementary Material

Refer to Web version on PubMed Central for supplementary material.

Acknowledgments

The computational work of this manuscript was supported in part by the National Institutes of Health (NIH 1S100D012346–01A1).

Abbreviations:

AMPs	antimicrobial peptides
CAms	cationic amphiphiles
CFU	colony-forming unit
MIC	minimum inhibitory concentration
CMC	critical micelle concentration
DLS	dynamic light scattering
SEM	scanning electron microscopy
TEM	transmission electron microscopy
hRBCs	human red blood cells
HFF	human foreskin fibroblast
MD	molecular dynamics

References

1. Aminov RI. A brief history of the antibiotic era: lessons learned and challenges for the future. *Front Microbiol* 2010;1:134. [PubMed: 21687759]
2. Giamarellou H Treatment options for multidrug-resistant bacteria. *Expert Rev Anti Infect Ther* 2006;4:601–18. [PubMed: 17009940]
3. Hancock REW, Lehrer R. Cationic peptides: a new source of antibiotics. *Trends Biotechnol* 1998;16:82–8. [PubMed: 9487736]
4. Findlay B, Zhanel GG, Schweizer F. Cationic amphiphiles, a new generation of antimicrobials inspired by the natural antimicrobial peptide scaffold. *Antimicrob Agents Chemother* 2010;54:4049–58. [PubMed: 20696877]
5. Guilhelmelli F, Vilela N, Albuquerque P, Derengowski L, Silva-Pereira I, Kyaw C. Antimicrobial development challenges: the various mechanisms of action of antimicrobial peptides and of bacterial resistance. *Front Microbiol* 2013;4. [PubMed: 23386843]
6. Zasloff M. Antimicrobial peptides of multicellular organisms. *Nature* 2002;415:389–95. [PubMed: 11807545]
7. Pushpanathan M, Gunasekaran P, Rajendhran J. Antimicrobial peptides: versatile biological properties. *Pept* 2013;2013, 675391.
8. Yeaman MR, Yount NY. Mechanisms of antimicrobial peptide action and resistance. *Pharmacol Rev* 2003;55:27–55. [PubMed: 12615953]
9. Cheng J, Chin W, Dong H, Xu L, Zhong G, Huang Y, et al. Biodegradable antimicrobial polycarbonates with in vivo efficacy against multidrug-resistant MRSA systemic infection. *Adv Healthc Mater* 2015;4:2128–36. [PubMed: 26331284]
10. Zhao J, Zhao C, Liang G, Zhang M, Zheng J. Engineering antimicrobial peptides with improved antimicrobial and hemolytic activities. *J Chem Inf Model* 2013;53:3280–96. [PubMed: 24279498]
11. Jiang L, Xu D, Sellati TJ, Dong H. Self-assembly of cationic multidomain peptide hydrogels: supramolecular nanostructure and rheological properties dictate antimicrobial activity. *Nanoscale* 2015;7:19160–9.
12. Yin LM, Edwards MA, Li J, Yip CM, Deber CM. Roles of hydrophobicity and charge distribution of cationic antimicrobial peptides in peptide-membrane interactions. *J Biol Chem* 2012;287:7738–45. [PubMed: 22253439]

13. Palermo EF, Vemparala S, Kuroda K. Cationic spacer arm design strategy for control of antimicrobial activity and conformation of amphiphilic methacrylate random copolymers. *Biomacromolecules* 2012;13:1632–41. [PubMed: 22475325]
14. Colak S, Nelson CF, Nüsslein K, Tew GN. Hydrophilic modifications of an amphiphilic Polynorbornene and the effects on its hemolytic and antibacterial activity. *Biomacromolecules* 2009;10:353–9. [PubMed: 19138065]
15. Palermo EF, Sovadinova I, Kuroda K. Structural determinants of antimicrobial activity and biocompatibility in membrane-disrupting Metha-crylamide random copolymers. *Biomacromolecules* 2009;10:3098–107. [PubMed: 19803480]
16. Liu SQ, Venkataraman S, Ong ZY, Chan JM, Yang C, Hedrick JL, et al. Overcoming multidrug resistance in Microbials using nanostructures self-assembled from cationic bent-Core oligomers. *Small* 2014;10:4130–5. [PubMed: 24975599]
17. Tang H, Doerksen RJ, Jones TV, Klein ML, Tew GN. Biomimetic facially amphiphilic antibacterial oligomers with Conformationally stiff backbones. *Chem Biol* 2006;13:427–35. [PubMed: 16632255]
18. Boughton AP, Andricioaei I, Chen Z. Surface orientation of Magainin 2: molecular dynamics simulation and sum frequency generation vibrational spectroscopic studies. *Langmuir* 2010;26:16031–6.
19. Scott RW, DeGrado WF, Tew GN. De novo designed synthetic mimics of antimicrobial peptides. *Curr Opin Biotechnol* 2008;19:620–7. [PubMed: 18996193]
20. Wieprecht T, Dathe M, Beyermann M, Krause E, Maloy WL, MacDonald DL, et al. Peptide hydrophobicity controls the activity and selectivity of Magainin 2 amide in interaction with membranes. *Biochemistry* 1997;36:6124–32. [PubMed: 9166783]
21. Chen Y, Guarnieri MT, Vasil AI, Vasil ML, Mant CT, Hodges RS. Role of peptide hydrophobicity in the mechanism of action of α -helical antimicrobial peptides. *Antimicrob Agents Chemother* 2007;51:1398–406. [PubMed: 17158938]
22. Abdelhamid DS, Zhang Y, Lewis DR, Moghe PV, Welsh WJ, Urich KE. Tartaric acid-based amphiphilic macromolecules with ether linkages exhibit enhanced repression of oxidized low density lipoprotein uptake. *Biomaterials* 2015;53:32–9. [PubMed: 25890704]
23. Faig A, Arthur TD, Fitzgerald PO, Chikindas M, Mintzer E, Urich KE. Biscationic tartaric acid-based amphiphiles: charge location impacts antimicrobial activity. *Langmuir* 2015;31:11875–85.
24. Zhang Y, Romsted LS, Zhuang L, de Jong S. Simultaneous determination of interfacial molarities of amide bonds, carboxylate groups, and water by chemical trapping in micelles of amphiphiles containing peptide bond models. *Langmuir* 2013;29:534–44. [PubMed: 23237147]
25. Torcato IM, Huang Y-H, Franquelim HG, Gaspar D, Craik DJ, Castanho MA, et al. Design and characterization of novel antimicrobial peptides, R-BP100 and RW-BP100, with activity against gram-negative and gram-positive bacteria. *Biochim Biophys Acta Biomembr* 2013;1828:944–55.
26. Joglekar M, Roggers RA, Zhao Y, Trewyn BG. Interaction effects of mesoporous silica nanoparticles with different morphologies on human red blood cells. *RSC Adv* 2013;3:2454–61.
27. Alhmoud H, Delalat B, Ceto X, Elnathan R, Cavallaro A, Vasilev K, et al. Antibacterial properties of silver dendrite decorated silicon nanowires. *RSC Adv* 2016;6:65976–87.
28. Spoden GA, Besold K, Krauter S, Plachter B, Hanik N, Kilbinger AF, et al. Polyethylenimine is a strong inhibitor of human papillomavirus and cytomegalovirus infection. *Antimicrob Agents Chemother* 2012;56:75–82. [PubMed: 21968369]
29. Dickson CJ, Madej BD, Skjervik ÅA, Betz RM, Teigen K, Gould IR, et al. Lipid14: the amber lipid force field. *J Chem Theory Comput* 2014;10:865–79. [PubMed: 24803855]
30. Molecular Operating Environment (MOE). 2013.08 ed. Chemical Computing Group, Inc.; 2016
31. Case DA, Betz RM, Botello-Smith W, Cerutti DS, Cheatham TE, Darden TA, et al. Amber 2015. San Francisco: University of California; 2015.
32. Hartmann M, Berditsch M, Hawecker J, Ardakani MF, Gerthsen D, Ulrich AS. Damage of the bacterial cell envelope by antimicrobial peptides gramicidin S and PGLa as revealed by transmission and scanning electron microscopy. *Antimicrob Agents Chemother* 2010;54:3132–42. [PubMed: 20530225]

33. Tang H, Lu A, Li L, Zhou W, Xie Z, Zhang L. Highly antibacterial materials constructed from silver molybdate nanoparticles immobilized in chitin matrix. *Chem Eng J* 2013;234:124–31.
34. Meer GV, Kroon AI. Lipid map of the mammalian cell. *J Cell Sci* 2010;124:5–8.
35. Oursel D, Loutelier-Bourhis C, Orange N, Chevalier S, Norris V, Lange CM. Lipid composition of membranes of *Escherichia coli* by liquid chromatography/tandem mass spectrometry using negative electrospray ionization. *Rapid Commun Mass Spectrom* 2007;21:1721–8. [PubMed: 17477452]
36. Maloy WL, Kari UP. Structure-activity studies on magainins and other host defense peptides. *Biopolymers* 1995;37:105–22. [PubMed: 7893944]
37. Zhang Y, Li Q, Welsh WJ, Moghe PV, Uhrich KE. Micellar and structural stability of nanoscale amphiphilic polymers: implications for anti-atherosclerotic bioactivity. *Biomaterials* 2016;84:230–40. [PubMed: 26828687]
38. Xu D, Jiang L, Singh A, Dustin D, Yang M, Liu L, et al. Designed supramolecular filamentous peptides: balance of nanostructure, cytotoxicity and antimicrobial activity. *Chem Commun* 2015;51:1289–92.
39. Rosen MJ, Mathias JH, Davenport L. Aberrant aggregation behavior in cationic gemini surfactants investigated by surface tension, interfacial tension, and fluorescence methods. *Langmuir* 1999;15:7340–6.
40. Laatiris A, El Achouri M, Infante MR, Bensouda Y. Antibacterial activity, structure and CMC relationships of alkanediyl α , ω -bis (dimethylammonium bromide) surfactants. *Microbiol Res* 2008;163:645–50. [PubMed: 17207986]
41. Li H, Yu C, Chen R, Li J, Li J. Novel ionic liquid-type gemini surfactants: synthesis, surface property and antimicrobial activity. *Physicochem Eng Asp* 2012;395:116–24.
42. Feder R, Dagan A, Mor A. Structure-activity relationship study of antimicrobial Dermaseptin S4 showing the consequences of peptide oligomerization on selective cytotoxicity. *J Biol Chem* 2000;275:4230–8. [PubMed: 10660589]
43. Torrent M, Valle J, Nogues MV, Boix E, Andreu D. The generation of antimicrobial peptide activity: a trade-off between charge and aggregation? *Angew Chem Int Ed* 2011;50:10686–9.
44. Li Y, Wu H, Teng P, Bai G, Lin X, Zuo X, et al. Helical antimicrobial Sulfonyl- γ -AApeptides. *J Med Chem* 2015;58:4802–11. [PubMed: 26020456]
45. Shai Y. Mode of action of membrane active antimicrobial peptides. *Pept Sci* 2002;66:236–48.
46. Wimley WC. Describing the mechanism of antimicrobial peptide action with the interfacial activity model. *ACS Chem Biol* 2010;5:905–17. [PubMed: 20698568]

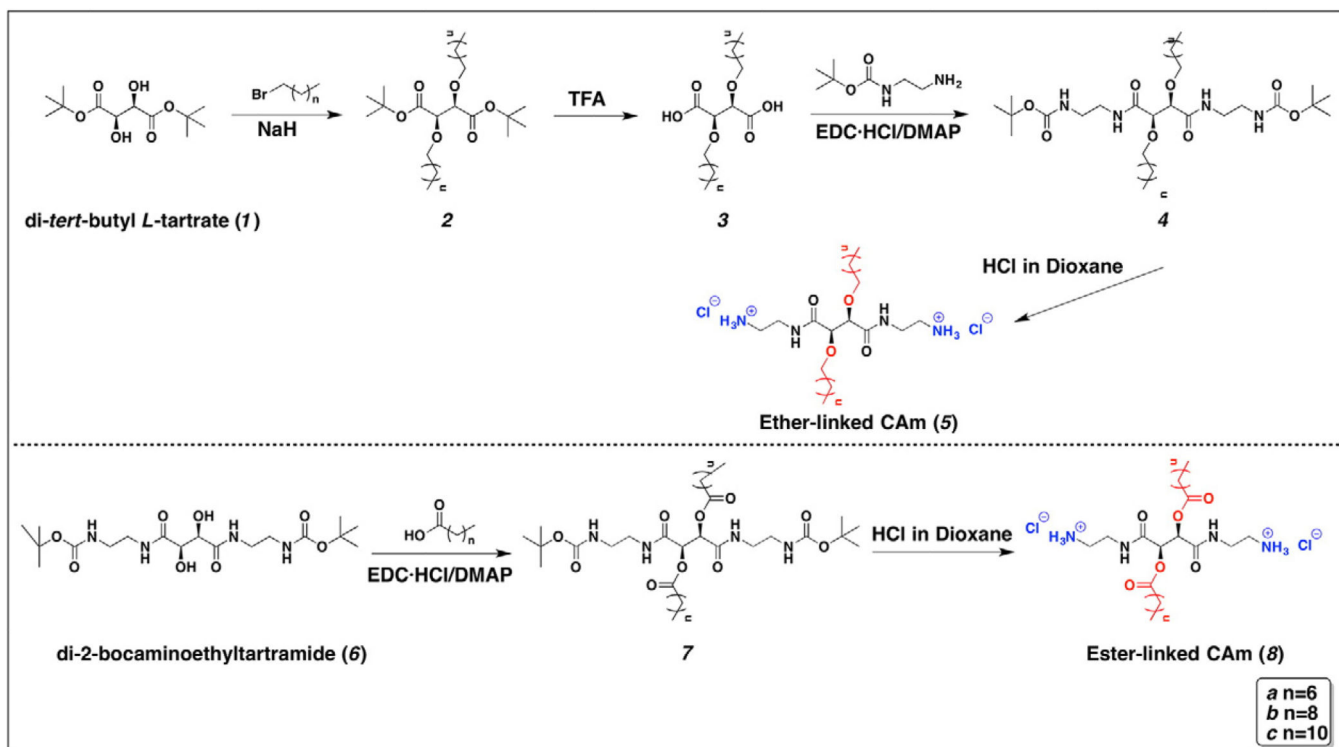


Figure 1.
Syntheses of ether- and ester-linked CAMs **5** and **8**.

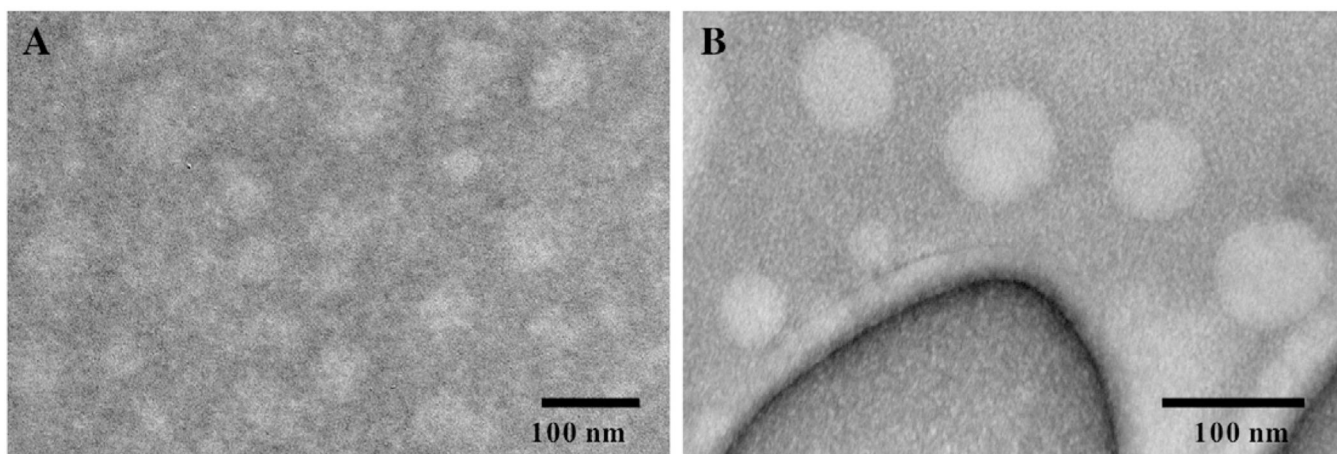


Figure 2. TEM images of representative supramolecular nanostructures formed by CAms *5b*(**A**) and *8b*(**B**) upon direct dissolution in water.

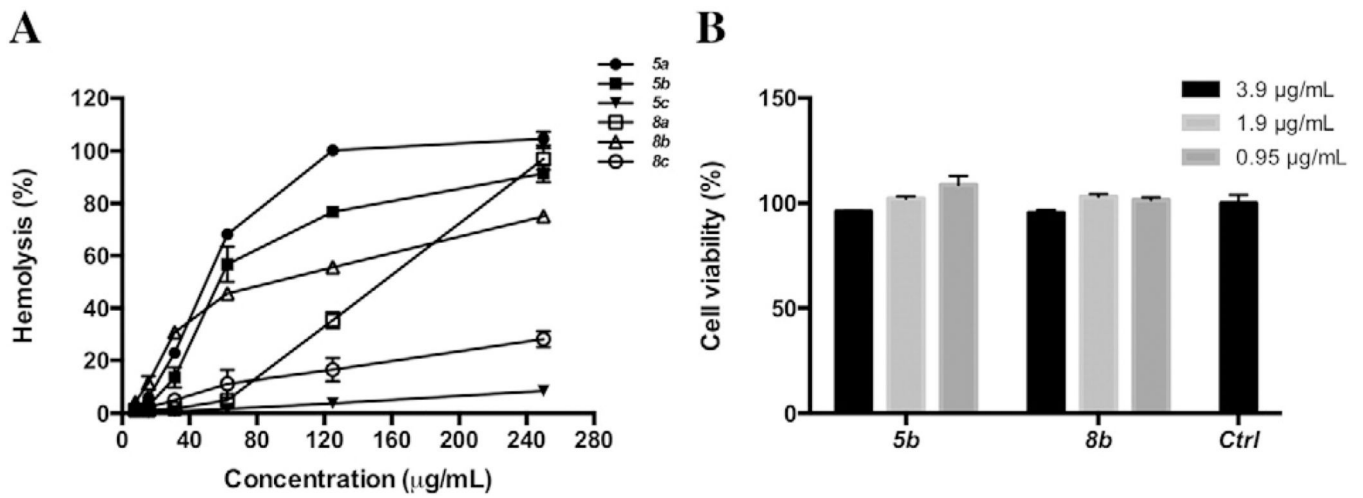


Figure 3. Hemolytic activities of CAMs at varied concentrations (A), and cytotoxicity of lead compounds *5b* and *8b* assessed by MTT assay (B) compared to medium only controls.

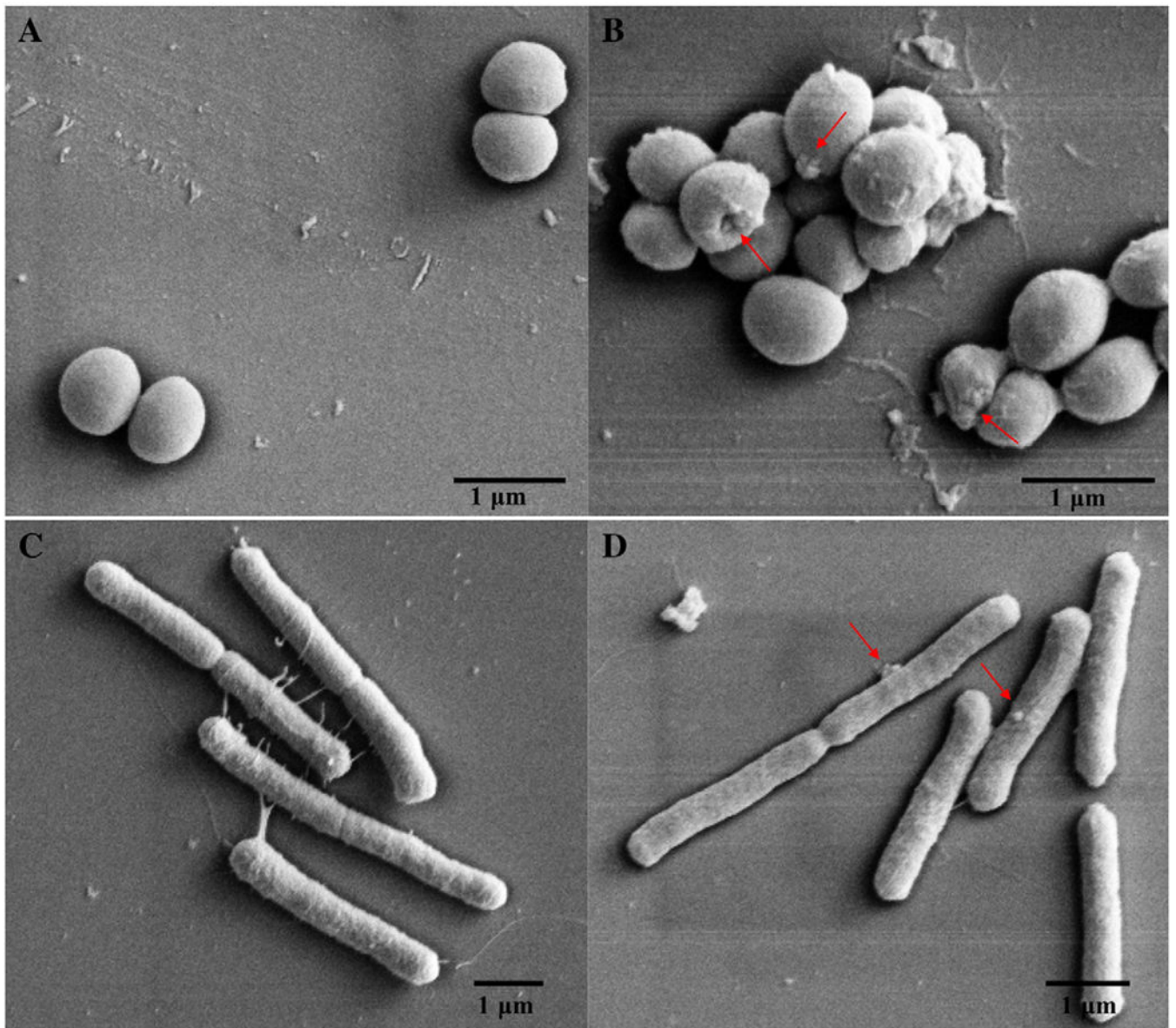


Figure 4. SEM micrographs of *S. aureus* and *E. coli* before (A, C) and after (B, D) incubation with 5b at their respective MICs. Varied morphological changes of cell membranes were indicated by red arrows.

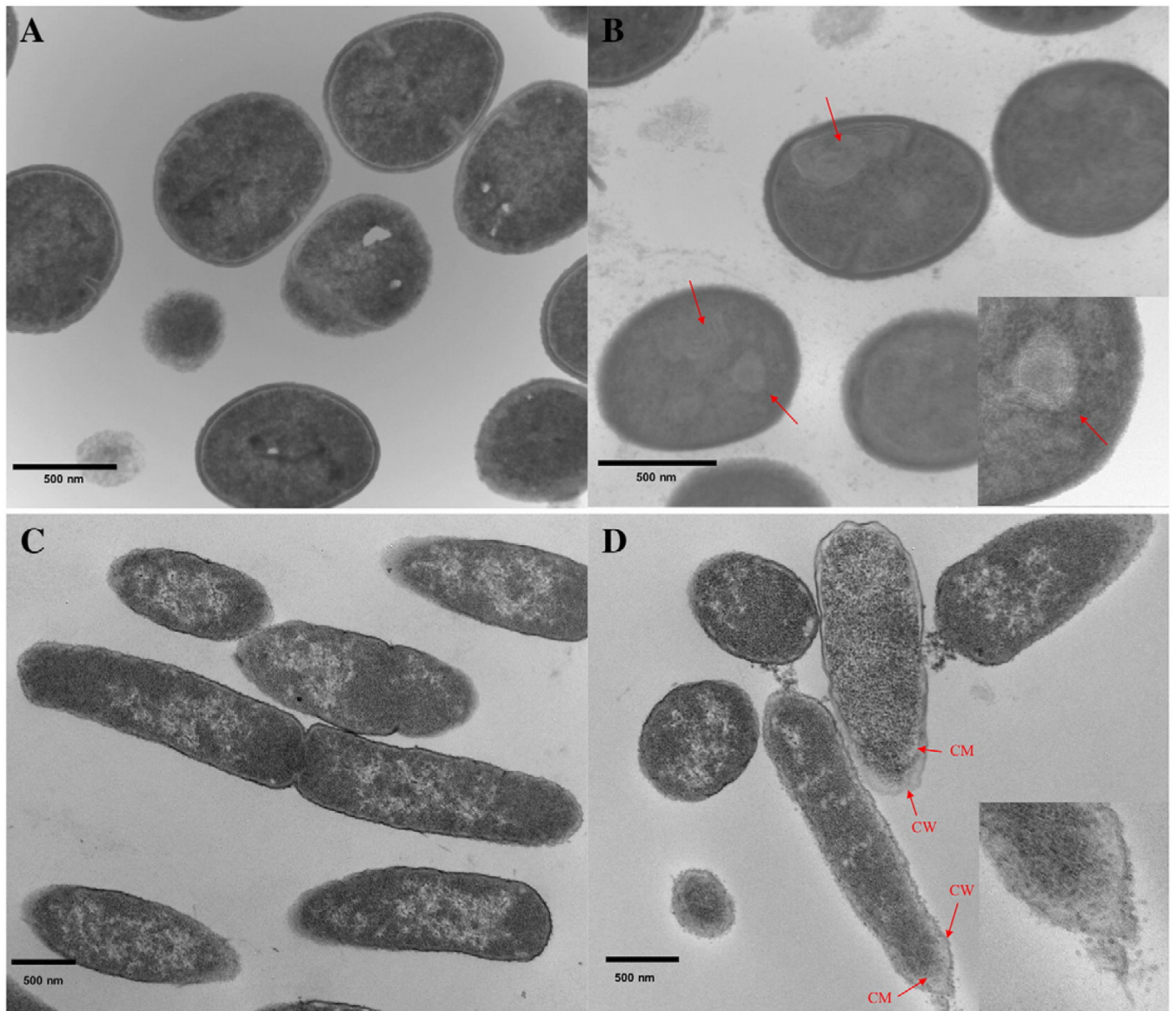


Figure 5. TEM micrographs of *S. aureus* and *E. coli* before (A, C) and after (B, D) incubation with 5b at their respective MICs. CW (cell wall or outer membrane), CM (cell inner membrane).

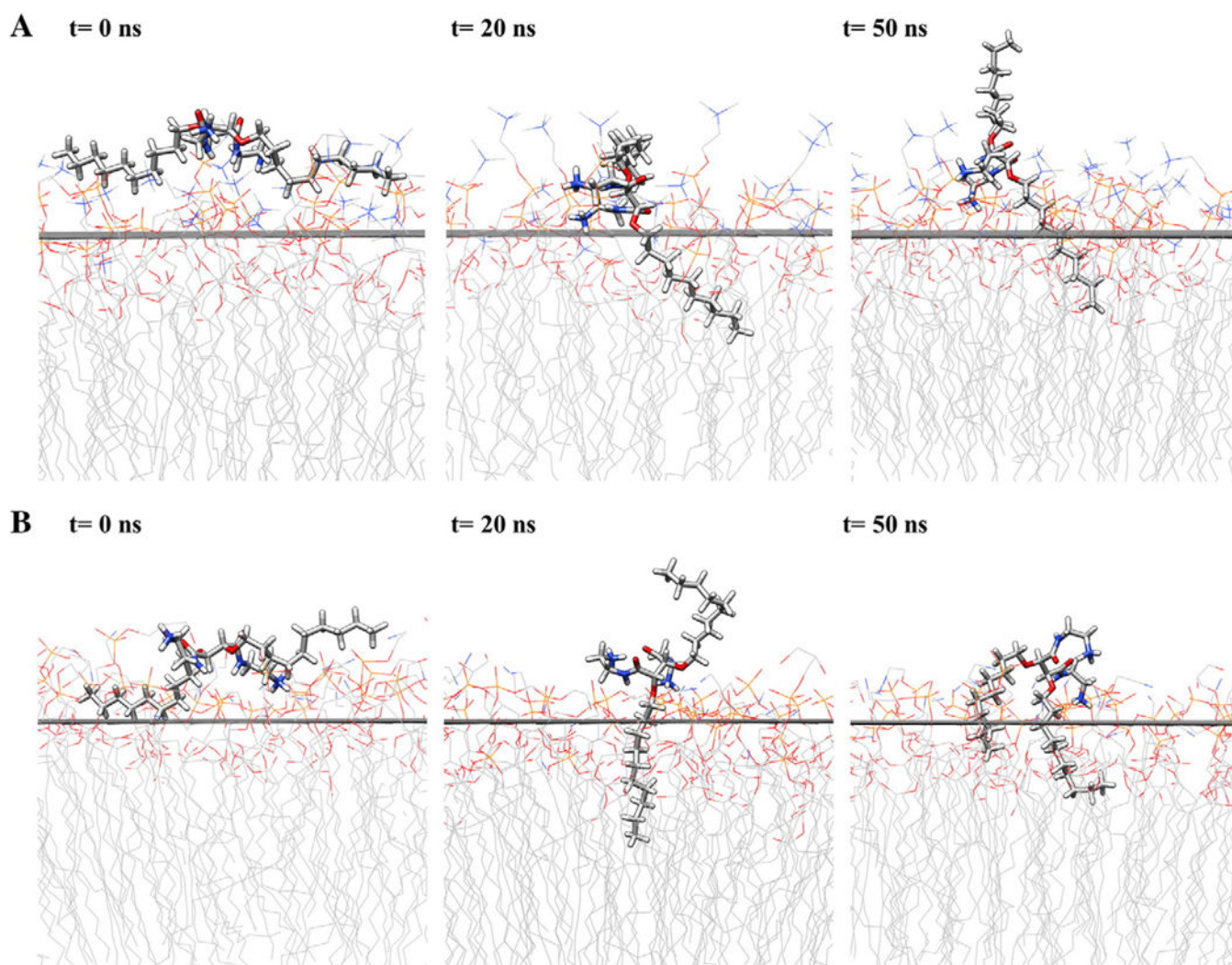


Figure 6. Snapshots along the simulation trajectory for mammalian membrane (**A**) and bacterial membrane (**B**) at time steps. Water and ions are not shown for clarity. Atoms are color-coded: C (gray), H (white), O (red), N (blue).

Table 1

Physicochemical and self-assembly properties of CAmS.

CAm	CMC ^a		Hydrodynamic Size ^a (nm)	PDI ^a	Zeta potential ^a (mV)
	($\mu\text{g/mL}$)	(mmol/L)			
5a	>1000	>1.88	n.a.	n.a.	n.a.
5b	110	0.187	53.7 \pm 3.0	0.21	21.3 \pm 1.3
5c	14	0.022	71.4 \pm 1.8	0.24	36.1 \pm 1.6
8a	>1000	>1.78	n.a.	n.a.	n.a.
8b	22	0.035	73.2 \pm 0.2	0.22	32.6 \pm 0.8
8c	4	0.006	104.9 \pm 0.4	0.19	44.8 \pm 2.7

Author Manuscript

Author Manuscript

Author Manuscript

Author Manuscript

Table 2

Antimicrobial and hemolytic activities of CAmS.

CAm	MIC ($\mu\text{g/mL}$)			HC ₅₀ ($\mu\text{g/mL}$)			SI	
	<i>S. aureus</i> (G+)	<i>L. monocytogenes</i> (G+)	<i>E. coli</i> (G-)	<i>S. typhimurium</i> (G-)	<i>P. aeruginosa</i> (G-)	G+	G-	
5a	3.9	3.9	15.6	7.8	3.9	12	3	
5b	0.95	0.95	3.9	3.9	3.9	68	17	
5c	3.9	125	>250	>250	>250	>250	n.a	
8a	31.2	31.2	62.5	62.5	31.2	4	2	
8b	1.9	1.9	3.9	3.9	3.9	43	21	
8c	15.6	>250	>250	>250	>250	>16	n.a	